An Overview of Level Set Methods for Etching, Deposition, and Lithography Development

James A. Sethian and David Adalsteinsson

Abstract—The range of surface evolution problems in etching, deposition, and lithography development offers significant challenge for numerical methods in front tracking. Level set methods for evolving interfaces are specifically designed for profiles which can develop sharp corners, change topology, and undergo orders of magnitude changes in speed. They are based on solving a Hamilton–Jacobi type equation for a level set function, using techniques borrowed from hyperbolic conservation laws. Over the past few years, a body of level set methods have been developed with application to microfabrication problems. In this paper, we give an overview of these techniques, describe the implementation in etching, deposition, and lithography simulations, and present a collection of fast level set methods, each aimed at a particular application. In the case of photoresist development and isotropic etching/deposition, *the fast marching level set method*, introduced by Sethian in [39], [40], can track the three-dimensional photoresist process through a $200 \times 200 \times 200$ rate function grid in under 55 s on a Sparc10. In the case of more complex etching and deposition, the *narrow band level set method*, introduced in Adalsteinsson and Sethian in [2], can be used to handle problems in which the speed of the interface delicately depends on the orientation of the interface versus an incoming beam, the effects of visibility, surface tension, reflection and re-emission, and complex three-dimensional effects. Our applications include photoresist development, etching/deposition problems under the effects of masking, visibility, complex flux integrations over sources, nonconvex sputter deposition problems, and simultaneous deposition and etch phenomena.

I. INTRODUCTION

IN THIS paper, we survey the use of level set methods for interface evolution problems in etching, deposition, and the photoresist development. The goal is accurate, stable, and efficient techniques for surface advancement due to complex motion which, under different physical effects, may include effects of anisotropy, visibility conditions, and material-dependent propagation rates. Level set methods are numerical techniques for tracking evolving interfaces which naturally handle and are specifically designed for profiles which can develop sharp corners, change topology, and undergo orders of magnitude changes in speed as they move. They are based on solving a Hamilton–Jacobi type equation for a level set function, using techniques borrowed from hyperbolic conservation laws.

In this paper, we present a collection of fast level set methods, each aimed at a particular application. In the case of photoresist development and isotropic etching/deposition, *the fast marching level set method*, introduced by Sethian in [39], [40], can track the three-dimensional photoresist process through a $200 \times 200 \times 200$ rate function grid in under 55 s on a Sparc10. In the case of more complex etching and deposition, the *narrow band level set method*, introduced in Adalsteinsson and Sethian [2], can be used to handle problems in which the speed of the interface delicately depends on the orientation of the interface versus an incoming beam, the effects of visibility, surface tension, reflection and re-emission, and complex three-dimensional effects.

A variety of numerical algorithms are available to advance fronts in etching, deposition and photolithography processes. These methods are not unique to such simulations, and in fact are in use in such areas as dendritic growth and solidification, flame/combustion models, and fluid interfaces. Roughly speaking, they fall into three general categories:

• *Marker/String Methods:* In these methods, a discrete parameterized version of the interface boundary is used. In two dimensions, marker particles are used; in three dimensions, a nodal triangularization of the interface is often developed. The positions of the nodes are then updated by determining front information about the normals and curvature from the marker representation. Such representations can be quite accurate, however, limitations exist for complex motions. To begin, if corners and cusps develop in the evolving front, markers usually form "swallowtail" solutions which must be removed through techniques which attempt to enforce an entropy condition inherent in such motion (see [33]). Second, topological changes are difficult to handle; when regions merge, some markers must be removed. Third, significant instabilities in the front can result, since the underlying marker particle motions represent a weakly ill-posed initial value problem (see [23]). Finally, extensions of such methods to three dimensions require additional work; for an application of marker particle methods to lithography problems, see [15].

• *Cell-Based Methods:* In these methods, see [22], the computational domain is divided into a set of cells which contain "volume fractions." These volume fractions are numbers between 0 and 1, and represent the fraction of each cell containing the physical material. At any time, the front can be reconstructed from these volume fractions. Advantages of such techniques include the ability to easily handle topological changes, adaptive mesh methods, and extensions to three dimensions. However, determination of geometric quantities

such as normals and curvature can be inaccurate. For a good review of such techniques, see [25].

• *Characteristic Methods:* In these methods, "ray-trace"-like techniques are used. The characteristic equations for the propagating interface are used, and the entropy condition at forming corners (see [33]) is formally enforced by constructing the envelope of the evolving characteristics. Such methods handle the looping problems more naturally, but may be complex in three-dimensions and require adaptive addition and removal of rays, which can cause instabilities and/or over smoothing.

Level set methods, introduced by Osher and Sethian in [23], offer a highly robust and accurate method for tracking interfaces moving under complex motions. Their major virtue is that they naturally construct the fundamental weak solution to surface propagation posed by Sethian [32], [33]. They work in any number of space dimensions, handle topological merging and breaking naturally, and are easy to program. They approximate the equations of motion for the underlying propagating surface, which resemble Hamilton–Jacobi equations with parabolic right-hand sides. The central mathematical idea is to view the moving front as a particular level set of a higher dimensional function. In this setting, sharp gradients and cusps can form easily, and the effects of curvature may be easily incorporated. The key numerical idea is to borrow the technology from the numerical solution of hyperbolic conservation laws and transfer these ideas to the Hamilton–Jacobi setting, which then guarantees that the correct entropy-satisfying solution will be obtained.

Since their introduction in [23], level set techniques have been used in a wide collection of problems involving moving interfaces. Some of these applications include the generation of minimal surfaces [10], singularities and geodesics in moving curves and surfaces in [11], flame propagation [27], [47], fluid interfaces [21], shape reconstruction [18], [19], as well as etching, deposition, and lithography calculations in [3], [4]. Extensions of the basic technique include fast methods in [2], level set techniques for multiple fluid interfaces and triple point junctions in [38], crystal growth [42], and grid generation in [36]. The fundamental Eulerian perspective presented by this approach has since been adopted in the theoretical analysis of mean curvature flow, in particular, see [9], [12].

The outline of this paper is as follows: In Section II, the theory of level set methods is described, with Sections II-A showing a time-dependent level set formulation, Section II-B showing a Stationary Time Level Set Formulation, and Section II-C showing shocks, entropy conditions, curvature, and viscosity. Section III, numerical schemes, shows approximations to the gradient (Section III-A), Fast narrow band methods for the time-dependent formulation (Section III-B), and Fast Marching Methods for the stationary formulation in Section III-C. Equations of Motion are given in Section IV. Applications are shown in Section V, with Section V-A describing photoresist development, Section V-B showing uni-directional and source deposition/etching: visibility, masking, etc.; Section V-C showing non-convex flux laws: sputter etching/deposition, and Section V-D presenting strongly discontinuous etch rates and simultaneous etching/deposition. Sections V-E–V-G show additional examples. Finally, Section VI has the summary and discusses future work.

II. THEORY OF LEVEL SET METHODS

Consider a boundary, either a curve in two dimensions or a surface in three dimensions, separating one region from another, and imagine that this curve/surface moves in its normal direction with a known speed function F. The goal is to track the motion of this interface as it evolves. We are only concerned with the motion of the interface in its normal direction, and shall ignore tangential motion. This speed F can depend on a variety of factors; typically, we can categorized them as

$$F = F(L, G, I) \qquad (1)$$

where

• L, *Local Properties of the front* are those determined by local geometric information, such as curvature and normal direction.

• G, *Global Properties of the front*, such as integrals along the front and associated differential equations, are those that depend on the shape and position of the front. For example, if the interface is a source of heat which affects diffusion on either side of the interface which in turn influences the motion of the interface, then this would be characterized as front-based argument.

• I, *Independent Properties* are those that are independent of the shape of the front, such as an underlying fluid velocity, which passively transports the front.

In terms of microfabrication problems, we can categorize some of the typical effects in terms of the above classification. For example,

• *Photoresist development* is an "independent property" speed function, since the speed function is only a function of position and supplied by an external calculation.

• *Surface diffusion and angle-dependent speed laws*, such as sputter deposition calculations, are "local properties," since the orientation of normal to the interface with respect to the incoming beam controls the front speed.

• *Visibility* is a "global property," since the position of the entire front affects the speed at each point.

Our goal is to assemble a single framework for looking at these problems.

A. A Time-Dependent Level Set Formulation

We now derive the level set formulation. Given an initial position for an interface Γ, where Γ is a closed curve in R^2, and a speed function F which gives the speed of Γ in its normal direction, the level set method takes the perspective of viewing Γ as the zero level set of a function $\phi(x, t = 0)$ from R^2 to R. That is, let $\phi(x, t = 0) = \pm d$, where d is the distance from x to Γ, and the plus (minus) sign is chosen if the point x is outside (inside) the initial hypersurface Γ. Then, by the chain rule, an evolution equation for the interface may be produced [23], [35], namely

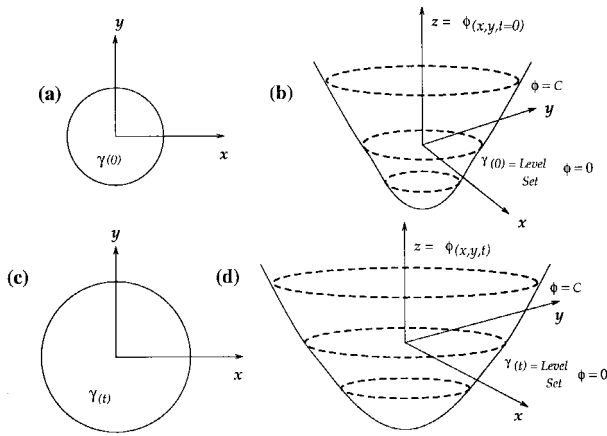$$\phi_t + F|\nabla \phi| = 0, \qquad (2)$$

Fig. 1. Propagating circle.

$$\phi(x, t = 0) = \text{given}, \qquad (3)$$

This is an initial value partial differential equation in one higher dimension than the original problem.[1] In Fig. 1 (taken from [36]), we show the outward propagation of an initial curve and the accompanying motion of the level set function ϕ. There are several advantages to this level set perspective:

1) Although $\phi(x, t)$ remains a function, the level surface $\phi = 0$ corresponding to the propagating hypersurface may change topology, as well as form sharp corners as ϕ evolves (see [23]).

2) Second, a discrete grid can be used together with finite differences to devise a numerical scheme to approximate the solution. Care must taken to adequately account for the spatial derivatives in the gradient.

3) Third, intrinsic geometric properties of the front are easily determined from the level set function ϕ. The normal vector is given by $\vec{n} = \nabla\phi/|\nabla\phi|$ and the curvature of each level set is $\kappa = \nabla \cdot \nabla\phi/|\nabla\phi|$.

4) Finally, the formulation is unchanged for propagating interfaces in three dimensions.

B. A Stationary Time Level Set Formulation

In the above level set equation

$$\phi_t + F|\nabla\phi| = 0 \qquad (4)$$

the position of the front is given by the zero level set of ϕ at a time t. Suppose we now restrict ourselves to the particular case of a front propagating with a speed F that is either always positive or always negative. In this case, we can convert our level set formulation from a time-dependent partial differential equation to a stationary one in which time has disappeared. We now describe the stationary level set formulation, given in [39], [40], and common in control theory.

To explain this transformation, imagine the two-dimensional case in which the interface is a propagating curve, and suppose we graph the evolving zero level set above the xy plane. That is, let $T(x, y)$ be the time at which the curve crosses the point

(x, y). The surface $T(x, y)$ then satisfies the equation

$$|\nabla T|F = 1. \qquad (5)$$

Equation (5) simply says that the gradient of arrival time surface is inversely proportional to the speed of the front. This is a form of the well-known Eikonal equation, which too is a Hamilton–Jacobi equation, and the recasting of the problem into a stationary one is common in a variety of applications, see [13], [14]. The requirement that the speed function always be positive[2] is so that the crossing time surface $T(x, y)$ is single-valued.

To summarize:

• In the time-dependent level set equation, the position of the front Γ at time t is given by the zero level set of ϕ at time t, that is $\Gamma(t) = \{(x, yt)|\phi(x, t) = 0\}$.

• In the stationary level set equation, the position of the front Γ is given by the level set of value t of the function $T(x, y)$, that is $\Gamma(t) = \{(x, y)|T(x, y) = t\}$.

What we shall see in the following section is that in both cases, the evolving curve/surface can develop corners where the evolving interface focuses, rarefaction fans where it expands, and regions where it changes topology. The key to constructing numerical schemes which correctly handle these mechanisms is to construct what are known as "entropy-satisfying" approximations to the gradient term in both (2) and (5).

C. Shocks, Entropy Conditions, Curvature, and Viscosity

As shown in [32], [33] and [35], a propagating interface can develop corners and discontinuities as it evolves, which requires the introduction of a weak solution in order to proceed. The correct weak solution comes from enforcing an entropy condition posed by Sethian [33] for the propagating interface, similar to the one in gas dynamics. Furthermore, this entropy-satisfying weak solution is the one obtained by considering the limit of smooth solutions for the problem in which curvature plays a regularizing role.

As an example, consider the initial cosine curve propagating with speed $F = 1$ shown in Fig. 2. As the front moves, a corner forms in the propagating front which corresponds to a shock in the slope, and a weak solution must be developed beyond this point. If the motion of each individual point is continued, the result is the swallowtail solution shown in Fig. 2(a), which is multiple-valued and does not correspond to a clear interface separating two regions. Instead, an appropriate weak solution is obtained by considering the associated smooth flow obtained by adding curvature κ to the speed law, that is, letting $F = 1 - \epsilon\kappa$, see Fig. 2(b). The limit of these smooth solutions as ϵ goes to zero produces the weak solution shown in Fig. 2(c).

Another way to obtain this same solution is through enforcing an entropy condition posed by Sethian [32], similar to the one for a scalar hyperbolic conservation law. Imagine that the front is the boundary of a propagating flame, separating a burning region below from an unburnt region above. The

---

[1] This is a particular form of the more general *Hamilton–Jacobi* equation which can be abstractly written as $\phi_t + H(\phi_x, \phi_y)$.

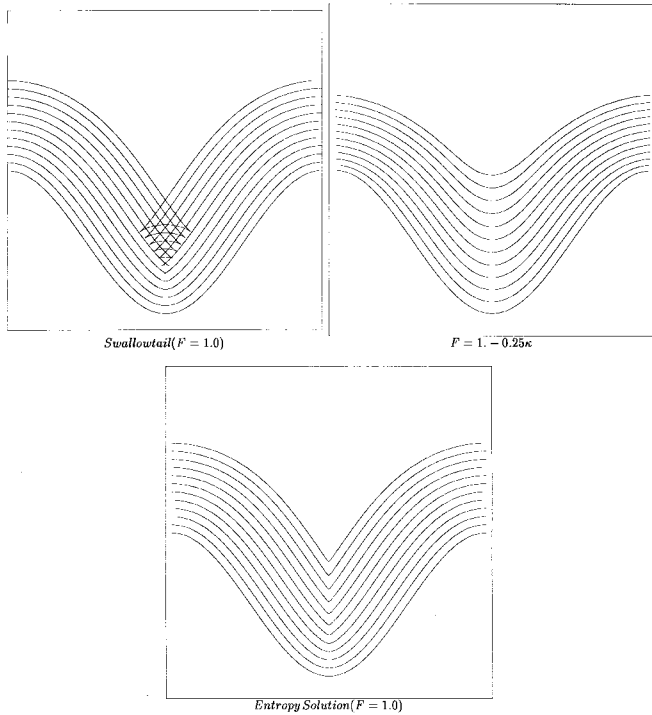[2] Or conversely, always negative

Fig. 2.   Cosine curve propagating with unit speed.

front at anytime t is the just the set of all points located a distance t from the initial front. Thus, the entropy condition may be stated briefly as "once a point burns, it stays burnt," see [32]. This weak solution corresponds to a decrease in total variation of the propagating front and is irreversible [33]. For details, see [33].

Since the entropy condition is similar to the one for hyperbolic conservation laws, as a numerical technique it suggests using that technology to solve the equations of motion, as described in [34].

III. NUMERICAL SCHEMES

Our goal is to solve both the time-dependent level set equation and the stationary level set equation for a front propagating with speed F, namely

Time-Dependent Formulation

$$\phi_t + F|\nabla \phi| = 0$$
$$\text{Front} = \Gamma(t) = \{(x, y)|\phi(x, yt) = 0\}$$
$$\text{Applies for arbitrary } F.$$

Stationary Formulation

$$|\nabla T|F = 1$$
$$\text{Front} = \Gamma(t) = \{(x, y)|T(x, y) = t\}$$
$$\text{Requires } F > 0. \tag{6}$$

In both cases, we require an "entropy-satisfying" approximation to the gradient term. In this next section, we discuss

appropriate approximations for this term, leading to schemes for both the time-dependent and stationary level set formulations.

A. Approximations to the Gradient

1) An Initial Attempt Using Central Differences: As motivation for approximating the gradient, we will study the simpler case of an evolving curve whose position can always be described as the graph of a function. Consider the initial front given by the graph of $f(x)$, with f and f' periodic on [0, 1], and suppose that the propagating front remains a function for all time. Let ψ be the height of the propagating function at time t, thus $\psi(x, 0) = f(x)$. The tangent at (x, ψ) is $(1, \psi_x)$. The change in height V in a unit time is related to the speed F in the tangent direction by

$$\frac{V}{F} = \frac{(1 + \psi_x^2)^{1/2}}{1} \tag{7}$$

and thus the equation of motion becomes $\psi_t = F(1 + \psi_x^2)^{1/2}$.

Suppose we approximate the solution by replacing all spatial derivatives with central differences and the time derivative with a forward difference. However, it is easy to see that such an algorithm may not work. Let $F = 1$ and consider the initial value problem

$$\psi_t = (1 + \psi_x^2)^{1/2},$$
$$\psi(x, 0) = f(x)$$
$$= \left\{ \begin{matrix} 1/2 - x & x \leq 1/2 \\ x - 1/2 & x > 1/2 \end{matrix} \right\}. \tag{8}$$

The initial front is a "V" formed by rays meeting at $(1/2, 0)$. By our entropy condition, the solution at any time t is the set of all points located a distance t from the initial "V." To construct a numerical scheme, divide the interval [0, 1] into $2M - 1$ points, and form the central difference approximation to the spatial derivative ψ_x in (8), namely

$$\psi_t \approx \frac{\psi_i^{n+1} - \psi_i^n}{\Delta t}$$
$$= \left[1 + \left(\frac{\psi_{i+1}^n - \psi_{i-1}^n}{2\Delta x} \right)^2 \right]^{1/2}$$
$$= [1 + (D_i^{0x}\psi)^2]^{1/2} \tag{9}$$

where in the last expression we have used standard notation for the central difference.

Since $x_M = 1/2$, by symmetry, $\psi_{M+1} = \psi_{M-1}$, thus the right-hand-side is 1. However, for all $x \neq 1/2$, ψ_t is correctly calculated to be $\sqrt{2}$, since the graph is linear on either side of the corner and thus the central difference approximation is exact. Note that this has nothing to do with the size of the space step Δx or the time step Δt. *No matter how small we take the numerical parameters, as long as we use an odd number of points, the approximation to ψ_t at $x = 1/2$ gets no better*. It is simply due to the way in which the derivative ψ_x is approximated. In Fig. 3 we show results using this scheme, with the time derivative ψ_t replaced by a forward difference scheme.
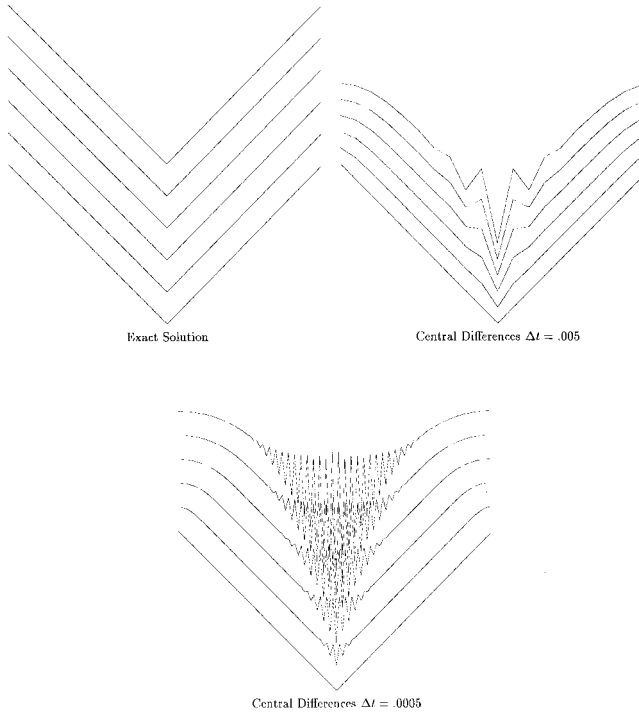
Fig. 3. Central difference approximation to level set equation.

(a)

(b)

Fig. 4. Upwind, entropy-satisfying approximations to the level set equation.

It is easy to see what has gone wrong. In the exact solution, $\psi_t = \sqrt{2}$ for all $x \neq 1/2$. This should also hold at $x = 1/2$ where the slope is not defined; the correct construction sets $\psi_t(x = 1/2, t)$ equal to $\lim_{x \to 1/2} \psi_t$. Unfortunately, the central difference approximation chooses a different (and, for our purpose, wrong) limiting solution. It sets the undefined slope ψ_x equal to the average of the left and right slopes. As the calculation progresses, this miscalculation of the slope propagates outwards from the spike as wild oscillations. Eventually, these oscillations cause blowup in the code.

2) Entropy-Satisfying Upwind Differences Schemes: We focus on the gradient term $(1 + \psi_x^2)$ (we call this a gradient term because ψ_x is the one-dimensional gradient). Consider now the following finite difference approximation introduced by Osher and Sethian [23]

$$\psi_x^2 \approx [\max (D_i^{+x}\psi, 0)^2 + \min (D_i^{-x}\psi, 0)^2] \quad (10)$$

where we have used standard finite difference notation that

$$D_i^{-x}\psi = \frac{\psi_i - \psi_{i-1}}{h}$$
$$D_i^{+x}\psi = \frac{\psi_{i+1} - \psi_i}{h} \quad (11)$$

where ψ_i is the value of ψ on a grid at the point ih with grid spacing h.

Equation (10) is an "upwind" scheme (see [41]); it chooses grid points in the approximation in terms of the direction of the flow of information. Intuitively, upwind means that if a wave progresses from left to right, then one should use a difference scheme which reaches *upwind* to the left in order to get information to construct the solution *downwind* to the right (see [41]). If we consider our propagating "V" curve from the example above, we see that at the symmetric point,
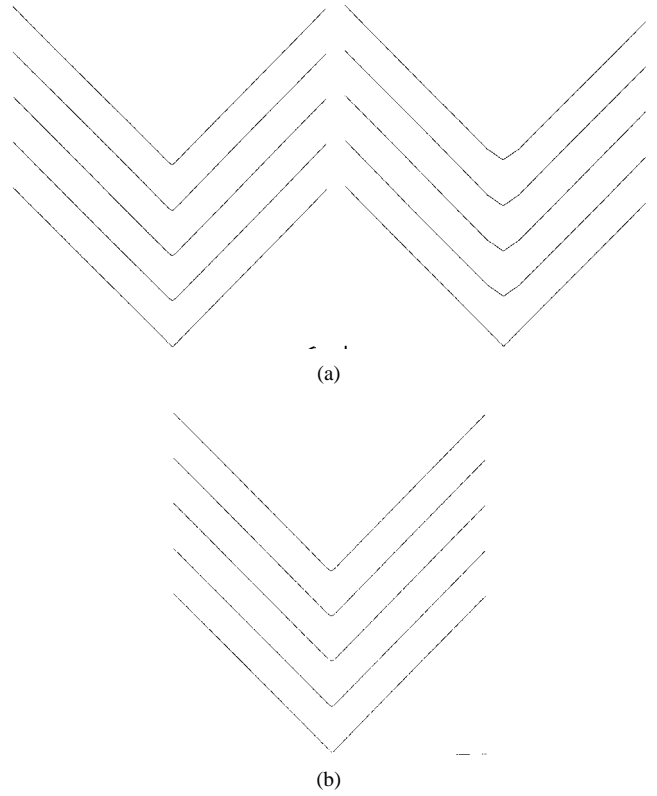
the symmetry of the scheme is changed, and a nonzero value is chosen. In Fig. 4, we show what happens if we use the scheme given in (10). The exact answer is shown, together with two simulations. The first uses the entropy-satisfying scheme with only 20 points [Fig. 4(b)], the second [Fig. 4(c)] with 100 points. In the first approximation, the entropy condition is satisfied, but the corner is somewhat smoothed due to the small number of points used. In the more refined calculation, the corner remains sharp, and the exact solution is very closely approximated. Thus we see that this scheme does a correct job of satisfying the entropy-condition.

While a vast array of other upwind, entropy-satisfying schemes are available to approximate the gradient, for our purposes, the above approximation (and one small variation) will be sufficient. More details on upwind schemes, hyperbolic conservation laws, and their role in level set equations may be found in [33], [40], and [41].

B. Schemes for Level Set Methods

Based on the above approximation to the gradient, we can now write down difference schemes for both of our level set methods. If one initializes the level set function with the signed distance function and ϕ negative on the inside, the direction of upwinding changes signs in the above approximation to the gradient, and we have (in three dimensions)

Solve:

• Time-Dependent Level Set Equation

$$\phi_{ijk}^{n+1} = \phi_{ijk}^n - \Delta t[\max (F_{ijk}, 0)\nabla^+ + \min (F_{ijk}, 0)\nabla^-] \quad (12)$$

where

$$\nabla^+ = [\max{(D_{ijk}^{-x}, 0)}^2 + \min{(D_{ijk}^{+x}, 0)}^2$$
$$+ \max{(D_{ijk}^{-y}\phi, 0)}^2 + \min{(D_{ijk}^{+y}\phi, 0)}^2$$
$$+ \max{(D_{ijk}^{-z}\phi, 0)}^2 + \min{(D_{ijk}^{+z}\phi, 0)}^2]^{1/2} \quad (13)$$

$$\nabla^- = [\max{(D_{ijk}^{+x}\phi, 0)}^2 + \min{(D_{ijk}^{-x}\phi, 0)}^2$$
$$+ \max{(D_{ijk}^{+y}\phi, 0)}^2 + \min{(D_{ijk}^{-y}\phi, 0)}^2$$
$$+ \max{(D_{ijk}^{+z}\phi, 0)}^2 + \min{(D_{ijk}^{-z}\phi, 0)}^2]^{1/2} \quad (14)$$

where $\phi(x, y, z, 0) = \pm d$.

- Stationary Time Level Set Equation

$$F_{ijk}[\max{(D_{ijk}^{-x}T, 0)}^2 + \min{(D_{ijk}^{+x}T, 0)}^2$$
$$+ \max{(D_{ijk}^{-y}T, 0)}^2 + \min{(D_{ijk}^{+y}T, 0)}^2$$
$$+ \max{(D_{ijk}^{-z}T, 0)}^2 + \min{(D_{ijk}^{+z}T, 0)}^2)] = 1 \quad (15)$$

where $T(x, y, z, 0) = 0$. Here, we avoided writing the difference approximation to the terms that influence the speed function F; see below.

The time-dependent method updates the level set function ϕ by advancing the solution one time step using a first order forward Euler scheme. This method can be made much faster through the use of so-called "narrow-band methods," introduced in [2]. The solution to the stationary equation is obtained by constructing a single solution to the problem, and can be made extremely fast in some special cases using a scheme introduced by Sethian in [39], [40] which marries the narrow-band methodology to a fast heapsort scheme with back pointers.

C. Fast Narrow Band Methods for the Time-Dependent Formulation

The time-dependent level set scheme above requires computing evolution of *all* the level sets, not simply the zero level set corresponding to the front itself. As such, it is a computationally expensive technique, since an extra dimension has been added to the problem.

As an alternative, an efficient modification is to perform work only in a neighborhood of the zero level set; this is known as the *narrow band approach*. In this case, the operation count in three dimensions for N^3 grid points drops to $O(kN^2)$, where k is the number of cells in the width of the narrow band, providing a significant cost reduction. This "narrow band method" method was introduced in [10], used in recovering shapes from images in [19], and analyzed extensively in [2].

The basic idea is to tag grid points as either "alive," "land mines," or "far away," depending on whether they are inside the band, near its boundary, or outside the band, respectively (see Fig. 5).

In Fig. 5, the black disks are "alive," the black disks on the edge of the band are "narrowband" points, and the open circles correspond to "far away" points. Instead of storing the full three-dimensional grid of points, a one-dimensional pointer array contains the value of the level set function and a pointer to its location in a three-dimensional space.
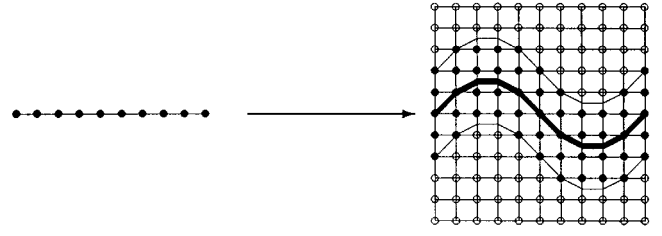

Fig. 5. Pointer array tags alive, narrow band, and far away points.

Thus, work is performed only on the alive points, and the band is reconstructed once land mine points are reached. There are several ways to perform this reconstruction, which is known as "re-initialization." One way is to find the new position of the front, and then simply recalculate the signed distance function around the new position, which yields a new narrow band. A variety of faster techniques are possible, and discussed in detail in [40] and [41].

Typically, this narrow band method is an order of magnitude faster than the full band level set method. In problems where calculations of additional effects such flux integration over the visible range of the source are important, the actual update of the level set portion using this narrow band technique requires an insignificant amount of computational labor.

D. Fast Marching Methods for the Stationary Formulation

An extreme one-cell version of this narrow band method leads to the fast marching level set method introduced by Sethian in [39], [40]. For ease of discussion, we limit ourselves to a two-dimensional problem inside a square from $[0, 1] \times [0, 1]$ and imagine that the initial front is along the line $y = 0$; furthermore, we assume that we are given a positive speed function $F(x, y)$ that is periodic in x. Thus, the front propagates upwards off the initial line, and the speed does not depend on the orientation of the front (it depends only on *independent variables*, using our earlier terminology). Using our approximation to the gradient, we are then looking for a solution in the unit box to the equation

$$F_{ij}[\max{(D_{ij}^{-x}T, 0)}^2 + \min{(D_{ij}^{+x}T, 0)}^2$$
$$+ \max{(D_{ij}^{-y}T, 0)}^2 + \min{(D_{ij}^{+y}T, 0)}^2)] = 1 \quad (16)$$

where $T(x, 0) = 0$.

Since (16) is in essence a quadratic equation for the value at each grid point (assuming the others are held fixed), we can iterate until convergence by solving the equation at each grid point, selecting the largest possible value as the solution in accordance with obtaining the correct viscosity solution. An iterative algorithm for computing the solution to this problem was introduced by Rouy and Tourin in [28]; there, a different approximation to the gradient was chosen which is less diffusive than the one given in [23], namely

$$F_{ij}\{\max{[\max{(D_{ij}^{-x}T, 0)}, -\min{(D_{ij}^{+x}T, 0)}]}^2$$
$$+ \max{[\max{(D_{ij}^{-y}T, 0)}, -\min{(D_{ij}^{+y}T, 0)}]}^2\} = 1.$$
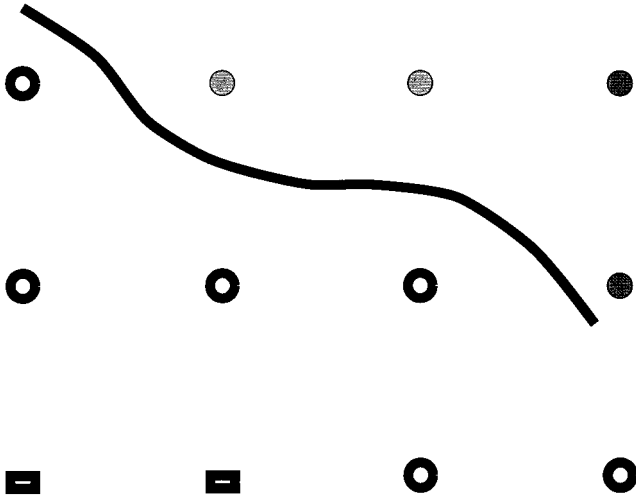$$\quad (17)$$

Fig. 6. Narrow band approach to marching level set method.

We shall use this approximation to the gradient in our fast marching level set method.

The key to constructing a fast marching algorithm is the observation that the upwind difference structure of (17) means that information propagates "one way," that is, from smaller values of T to larger values. Hence, our algorithm rests on "solving" (17) by building the solution outwards from the smallest time value T. The idea in [40] is to sweep the front ahead in an upwind fashion by considering a set of points in narrow band around the existing front, and to march this narrow band forward, freezing the values of existing points and bringing new ones into the narrow band structure. The key is in the selection of *which* grid point in the narrow band to update. The technique is easiest to explain algorithmically, see Fig. 6, taken from [40]. We imagine that we want to propagate a front downwards through an $N \times N$ grid with speed F_{ij} giving the speed in the normal direction at each grid point. Here the set of grid points $j = N$ correspond to the y axis, and we assume that $F_{ij} > 0$.

Algorithm:

1) Initialize

   a) (Alive Points: Grey Disks): Let A be the set of all grid points $\{i, j = N\}$; set $T_{i, N} = 0.0$ for all points in A.

   b) (Narrow Band Points: Black Circles): Let *Narrow Band* be the set of all grid points $\{i, j = N\}$, set $T_{i, 1} = dy/F_{ij}$ for all points in *Narrow Band*.

   c) (Far Away Points: Black Rectangles): Let *Far Away* be the set of all grid points $\{i, j < N - 1\}$, set $T_{i, j} = \infty$ for all points in *Far Away*.

2) Marching Forward

   a) Begin Loop: Let $(i_{\min}, j_{\min})$ be the point in *Narrow Band* with the smallest value for T.

   b) Add the point $(i_{\min}, j_{\min})$ to A; remove it from *Narrow Band*.

   c) Add to the narrow band list any neighboring points $(i_{\min} - 1, j_{\min})$, $(i_{\min} + 1, j_{\min})$, $(i_{\min}, j_{\min} - 1)$,

$(i_{\min}, j_{\min} + 1)$ that are not *Alive*. If the neighbor is in *Far Away*, remove it from that list.

   d) Recompute the values of T at all neighbors according to (17), selecting the largest possible solution to the quadratic equation.

   e) Return to top of Loop.

We take periodic boundary conditions where required. Assuming for the moment that it takes no work to determine the member of the narrow band with the smallest value of T, the total work required to compute the solution at all grid points is $O(N^2)$, where calculation is performed on an $N \times N$ grid.

Why does the above algorithm work? Since we are always locating the smallest value in the narrow band, its value for T must be correct; other narrow band points or far away points with larger T values cannot affect it. The process of recomputing the T values at neighboring points (that have not been previously accepted) cannot yield a value smaller than any of that at any of the accepted points, since the correct viscosity solution is obtained by selecting the *largest* possible solution to the quadratic equation. Thus, we can march the solution outwards, always selecting the narrow band grid point with minimum trial value for T, and readjusting neighbors. Another way to look at this is that each minimum trial value begins an application of Huygen's principle, and the expanding wave front touches and updates all others. A formal proof of the convergence of the algorithm to the correct solution may be found in [39].

1) Finding the Smallest Value: The key to an efficient version of the above technique lies in a fast way of locating the grid point in the narrow band with the smallest value for T. We use a variation on a heapsort algorithm, see Press *et al.* [24] and Sedgewick [31], with the additional feature of back pointers. In more detail, imagine that the list of narrow band points is initially sorted in a heapsort so that the smallest member can be easily located. We store the values of these points in the heapsort, together with their indices which give their location in the grid structure. We keep a companion array which points from the two-dimensional grid to the location of that grid point in the heapsort array. Finding the smallest value is easy. In order to find the neighbors of that point, we use the pointers from the grid array to the heapsort structure. The values of the neighbors are then recomputed, and then the results are bubbled upwards in the heapsort until they reach their correct locations, at the same time readjusting the pointers in the grid array. This results in an $O(\log N)$ algorithm for the total amount of work, where N is the number of points in the narrow band. For implementation details and further application of this technique, see [1], [39], and [40].

E. Some Clarifying Comments

The time-dependent level set method and the stationary level set method each require careful construction of upwind, entropy-satisfying schemes, and make use of the dynamics and geometry of front propagation analyzed in [33]. However, we note that the time-dependent level set method advances the front **simultaneously**, while the stationary method constructs "scaffolding" to build the time solution surface T one grid

point at a time. This means that the time at which the surface crosses a grid point (that is, its T value) may be found before other positions of that front at that time are determined. As such, there is **no** notion of a time step in the stationary method; one is simply constructing the stationary surface in an upwind fashion.

This means that if one is attempting to solve a problem in which the speed of a front depends on the current position of the front (such as in the case of visibility), or on subtle orientations in the front (such as in sputter yield problems), it is not clear how to use the stationary method, since the front is being constructed one grid point at a time. In the case where speed F only depends on independent variables, such as in the case of photolithography development, the implementation of the fast marching method is straightforward. Upwind entropy-satisfying schemes which can be transported to this fast stationary scheme for the case of more general speed functions F are more problematic, and discussed in detail in [1], [41].

To summarize:

- The stationary method is convenient for problems in which the front speed depends on independent variables, such as a photoresist rate function, and only applies if the speed function does not change sign.
- The time-dependent level set method is designed for more delicate speed functions, and can accurately fronts evolving under highly complex arguments.

F. Non-Convex Speed Laws

Our approximations to the gradient only work for *convex* speed functions. We will need a modification in the case of *nonconvex* speed functions, which will turn out to be of critical importance in some problems of interest in etching and deposition. In this brief section, we define some of these terms, and explain the necessary modifications, for details, see [41].

We focus again on our time-dependent level set equation, namely

$$\phi_t + F|\nabla\phi| = 0. \tag{18}$$

We rewrite this as

$$\phi_t + H(\nabla\phi) = 0. \tag{19}$$

where the "Hamiltonian" $H = F|\nabla\phi|$.

To make things clear, we focus on the one-dimensional case, in which we have that $H = F(\phi_x)|\phi_x|$, where we have included the possible dependence of the speed function F on the derivative of ϕ. We say that such a Hamiltonian is convex if $d^2H/dx^2 < 0$.[3] If F does not depend on ϕ [which is the case in photoresist development and isotropic etching and deposition, see Fig. 7(a)], then it is easy to see that H is convex. Our approximations to the gradient are specifically constructed for convex Hamiltonians; that is, at points where
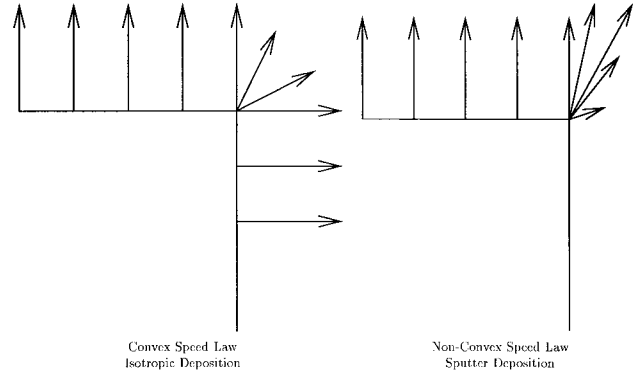
Fig. 7. Contrast of convex versus nonconvex speed laws.

the derivative does not exist, a careful blending of values from the left state and the right state results.

Now, suppose H is not convex. A simple example of a nonconvex speed function is provided in sputter deposition, in which a speed function F may depend on the angle θ between the normal and an incoming beam in such a way that the maximal speed occurs at a value between 0 and $\pi/2$, see Fig. 7(b). In this case, our scheme fails at places where the front has corners.

Intuitively, the reason nonconvex speed functions are difficult is because where the front has a corner, it is difficult to simply combine the speed on the left and the speed on the right to get a "good" value for the range of possible speeds in between.

The simplest way of constructing difference approximation which account for nonconvex speed laws is to go back to our idea of a viscosity solution, and simply "smooth out" the corners so that sharp corners cannot occur. With sophisticated schemes (see [3] and [4]), the amount of smoothing can be limited to a few grid cells.

Thus, a level set scheme which smoothes the corners is based on a Lax–Friedrichs method, and is given by [3] and [4]

$$\phi_{ijk}^{n+1} = \phi_{ijk}^n - \Delta t \left[H\left(\frac{D_{ijk}^{-x} + D_{ijk}^{+x}}{2}, \right. \right.$$
$$\left. \frac{D_{ijk}^{-y} + D_{ijk}^{+y}}{2}, \frac{D_{ijk}^{-z} + D_{ijk}^{+z}}{2} \right)$$
$$- \tfrac{1}{2}\alpha_u(D_{ijk}^{+x} - D_{ijk}^{-x}) - \tfrac{1}{2}\alpha_v(D_{ijk}^{+y} - D_{ijk}^{-y})$$
$$\left. - \tfrac{1}{2}\alpha_w(D_{ijk}^{+z} - D_{ijk}^{-z}) \right] \tag{20}$$

where α_u (α_v, α_w) is a bound on the partial derivative of the Hamiltonian with respect to the first (second, third) argument, and the nonconvex Hamiltonian is a user-defined input function. The terms on the second row of the above are the smoothing terms, and resemble second derivatives in each variable (i.e., $\phi_{x}x$); the amount of smoothing is proportional to the grid spacing.

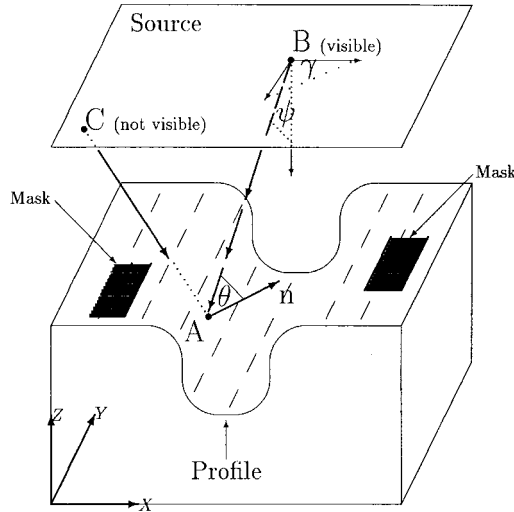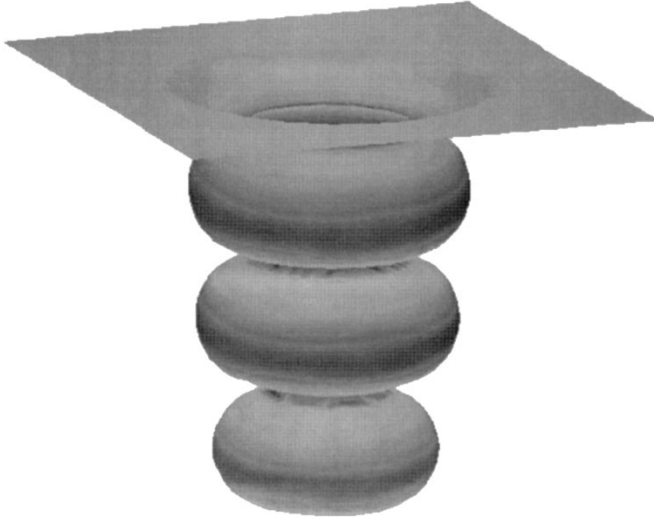We will need this scheme when we tackle complex sputter deposition and etching problems.

Fig. 8.   Variables and setup.

Fig. 9.   Lithographic development on $50 \times 50 \times 50$ grid.

IV. EQUATIONS OF MOTION

A. Layout of Variables

In this section, we produce equations of motion. Excellent overviews describing these physical effects may be found in Scheckler [29], Scheckler, Toh, Hoffstetter and Neureuther [30], Toh [45], and Toh and Neureuther [46], see also Rey, Cheng, McVittie, and Saraswat [26], McVittie, Rey, Bariya *et al.* [20], Cale and Raupp [6]–[8], and Singh [43].

For both etching and deposition, define the source ray to be the ray leaving the source and aimed toward the surface profile. Let ψ be the angle variation in the source ray away from the negative z axis; ψ runs from 0 to π, though it is physically unreasonable to have ϕ values between $\pi/2$ and π. Let γ be the angle between the projection of the source ray in the xy plane and the positive x axis. Let n be the normal vector at a point x on the surface profile, and θ the angle between the normal and the source ray. In Fig. 8, we indicate these variables. Masks, which force flux rates to be zero, are indicated by heavy dark patches on the initial profile. At each point of the profile, we also assign a visibility indicator function $M_\Upsilon(\vec{x}, \vec{x}')$ which

indicates whether the point $\vec{x}$ on the initial profile can be seen by the source point $\vec{x}'$.

Ignoring lithography development for the moment, we may, somewhat abstractly, write a single general expression for the effects of deposition and etching on the speed F at a point $\vec{x}$ on the front as

$$F = F_{Iso}^{Etch} + F_{Dir}^{Etch} + F_{Iso}^{Dep} + F_{Dir}^{Dep} + F_{Re\text{-}Dep}^{Dep} + F_{Re\text{-}Em}^{Dep} \tag{21}$$

where

- $F_{Isotropic}^{Etching}$: *Isotropic etching.* Uniform (chemical or "wet") etching.
- $F_{Direct}^{Etching}$: *Direct etching from an external source (includes visibility)*
- F_{Iso}^{Dep}: *Isotropic deposition.*
- F_{Dir}^{Dep}: Direct deposit ion from an external source (includes visibility).
- $F_{Re\text{-}Dep}^{Dep}$: *Ion-induced Re-deposition sticking coefficient* $\beta_{re\text{-}deposition}$.
- $F_{Re\text{-}Em}^{Dep}$: *Re-emission deposition: sticking coefficient* $\beta_{re\text{-}emission}$.

The two isotropic terms are evaluated at a point x by simply evaluating the strengths at that point. The two direct terms are evaluated at a point x on the profile by first computing the visibility to each point of the source, and then evaluating the flux function; thus these terms require computing an integral over the entire source. To compute the fifth term at a point x, the contributions of every point on the profile are checked for re-deposition particles arising from the etching process, thus this term requires computing an integral over the profile itself. The sixth term, $F_{Re\text{-}Em}$ is more problematic; since every point on the front can act as a deposition source of re-emitted particles that do not stick, the total flux function deposition function comes from evaluating an integral equation along the entire profile.

In more detail, let Ω be the set of points on the evolving profile at time t, and let So be the external source. Given two points $\vec{x}$ and $\vec{x}'$, let $M_\Upsilon(\vec{x}, \vec{x}')$ be one if the points are visible from one another and zero otherwise. Let r be the distance from x to x', $\vec{n}$ be the unit normal vector at the point x, and finally, let $\vec{\alpha}$ be the unit vector at the point $\vec{x}'$ on the source pointing toward the point x on the profile. Then we may refine the above terms for the flux FL as

$$F = \left[FL_{Iso}^{Etch} + \int_{So} FL_{Dir}^{Etch}(r, \psi, \gamma, \theta, \vec{x}) \right.$$
$$\cdot M_{\Upsilon(\vec{x}, \vec{x}')}(\vec{n} \cdot \vec{\alpha}) \, d\vec{x}' + FL_{Iso}^{Dep}$$
$$+ \int_{So} FL_{Dir}^{Dep}(r, \psi, \gamma, \theta, \vec{x}) M_{\Upsilon(\vec{x}, \vec{x}')}(\vec{n} \cdot \vec{\alpha}) \, d\vec{x}'$$
$$+ \int_{\Omega} \beta_{re\text{-}dep} FL_{Re\text{-}dep}^{Dep}(r, \psi, \gamma, \theta, \vec{x})$$
$$\cdot M_{\Upsilon(\vec{x}, \vec{x}')}(\vec{n} \cdot \vec{\alpha}) \, d\vec{x}'$$
$$+ \int_{\Omega} \beta_{re\text{-}em} FL_{Re\text{-}em}^{Dep}(r, \psi, \gamma, \theta, \vec{x})$$
$$\left. \cdot M_{\Upsilon(\vec{x}, \vec{x}')}(\vec{n} \cdot \vec{\alpha}) \, d\vec{x}' \right]. \tag{22}$$

Grid Size	50^3	100^3	150^3	200^3	Exact
Exit T_{final}	9.809	10.339	10.366	10.367	10.367
Rel. Error	.05387	.00268	.00014	.00008	0.0
Compute Time	.5 secs	5.0 secs	20.0 secs	55. secs	–

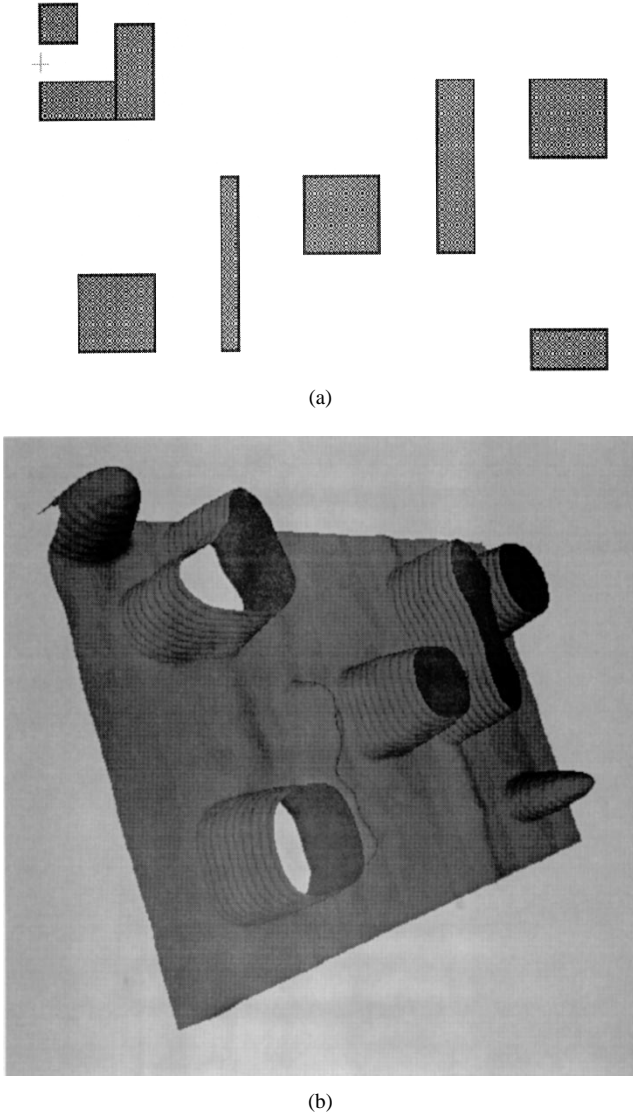Fig. 10.   Timings and accuracy as a function of grid size.

(a)

(b)

Fig. 11.   Lithographic development using fast marching method.

(a)

(b)

Fig. 12.   Isotropic etching into hole.

direct deposition. Thus, as presented, this last term requires N^2 evaluations, where N is the number of control points which approximate the front. This requires the solution of a matrix equation for a matrix M which is nonsymmetric and full. Details may be found in [5].

V. RESULTS: APPLICATIONS

In this section, we show a series of results using the above level set methods for problems in etching, deposition, and photoresist development. All calculations are taken from [3]–[5], and [39].

A. Lithographic Development

As a first example, we use the fast marching level set method introduced by Sethian [39], [40] for the stationary level set equation to compute a lithographic development profile for an evolving front. We start with a flat profile at height $z = 1$ in the unit cube centered at (0.5, 0.5, 0.5) and follow the evolution of the interface downwards with speed given by the model Gaussian rate function

$$F(x, y, z) = e^{-64(r^2)} \left[\cos^2(12z) + 0.01\right] \qquad (23)$$

where $r = \sqrt{(x - 0.5)^2 + (y - 0.5)^2}$. This rate function F corresponds to effect of standing waves which change the resist

The integrals are performed in a straightforward manner. The front is located by constructing the zero level set of ϕ; in two dimensions it is represented by a collection of line segments; in three-dimensions by a collection of voxel elements, see [3] and [4]. The centroid of each element is taken as the control point, and the individual flux terms are evaluated at each control point. In the case of the two isotropic terms, the flux is immediately found. In the case of the two integrals over sources, the source is suitably discretized and the contributions summed. In the fifth term, corresponding to re-deposition, the integral over the entire profile is calculated by computing the visibility to all other control points and the corresponding re-deposition term produced by the effect of
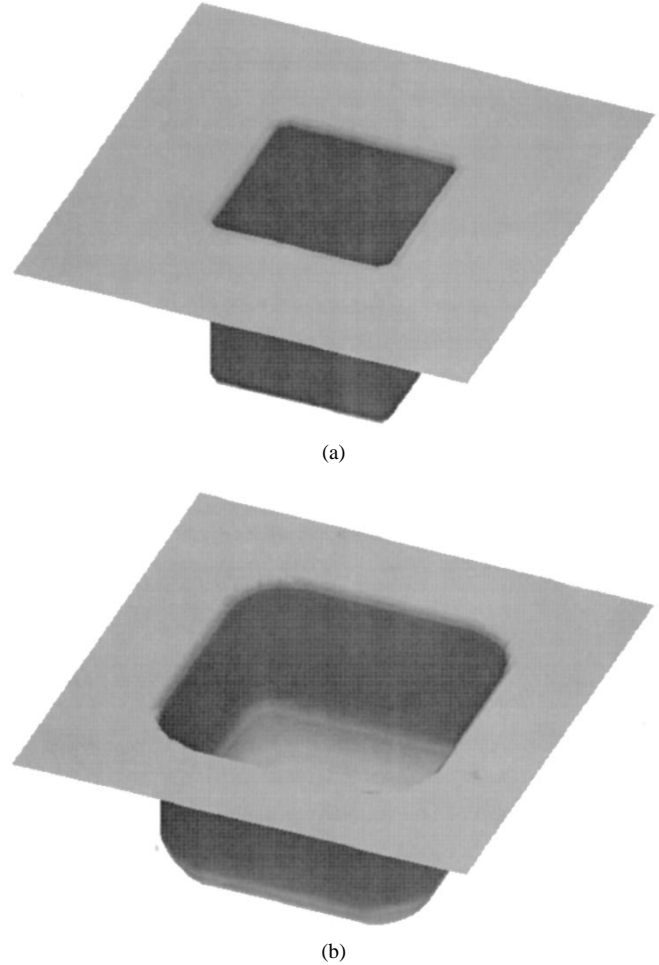
T=0.0 T=2.0 T=3.0
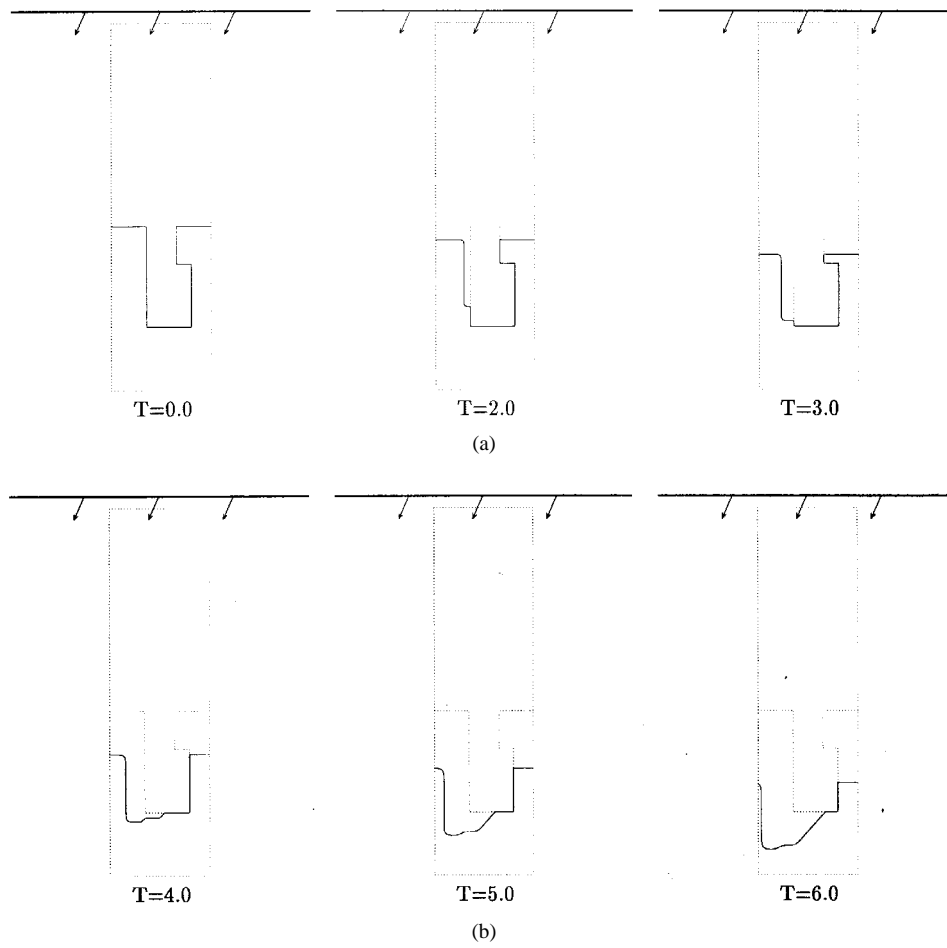
(a)

T=4.0 T=5.0 T=6.0

(b)

Fig. 13. Directional etching into cavity.

properties of the material, and causes sharp undulations and turns in the evolving profile. In Fig. 9, see [39], we show the profile etched out by such an initial state; the calculation is carried out until $T = 10$.

Fig, 10 shows timings and errors for speed function $F = e^{-64(r^2)}[\cos^2(6z) + 0.01]$. Here, $ExitT_{final}$ is the time when the profile exits the bottom, $RelativeError = |Computed - Exact|/Exact$, and $ComputeTime$ is the time to develop the front until T_{final} on a Sparc 10.

As a second example, we use the masking pattern given in Fig. 11(a) using an I-line stepper, numerical aperture 0.6. The rate function is calculated using the three-dimensional exposure and post-exposure bake modules of Depict 4.0 [44], and this is coupled to our fast marching level set method. In Fig. 11(b), see [41], we show a view of the developed profile looking up from underneath; the etching of the holes and the presence of standing waves can easily be seen.

B. Isotropic, Uni-Directional, and Source Deposition/Etching

1) Isotropic Etching/Deposition: Next, we study some etching and deposition simulations. In Fig. 12 we show a square hole from which a material is being isotropically etched; this corresponds to a simple speed function of $F = -1$. This could be performed using either the stationary solution or the time-dependent technique, since the speed depends only an

independent variables; the simulation shown uses the narrow band time-dependent technique. As expected, the sides of the cavity are cleanly etched away, leaving smoothed, rounded walls.

2) Directional Etching/Deposition: Next, we show some examples of uni-directional etching/deposition. Here, the particles come from a single direction, and the effects of visibility are included, thus, the time-dependent level set technique is used.

We begin with a two-dimensional example of directional etching. Material emits from the line source at an angle of $30°$ from the vertical. In Fig. 13, we show results at various times, starting with the initial state. There is no yield variation in the etch rate due to angle of incidence with the normal. In other words, the speed of the profile in the normal direction is just the projection of the directional etch rate in that normal direction. Due to the effects of shadowing, as the profile evolves we again see that part of the profile aligns itself tangential to the incoming unidirectional etching stream.

A three-dimensional simulation is shown in Fig. 14. We consider directional etching from a plate located above a square hole, where the effects of visibility and shading are included. We show a sequence of three-dimensional time plots which show the evolving profile. The etching direction is on the upper right in the figure; the etching beam shears away
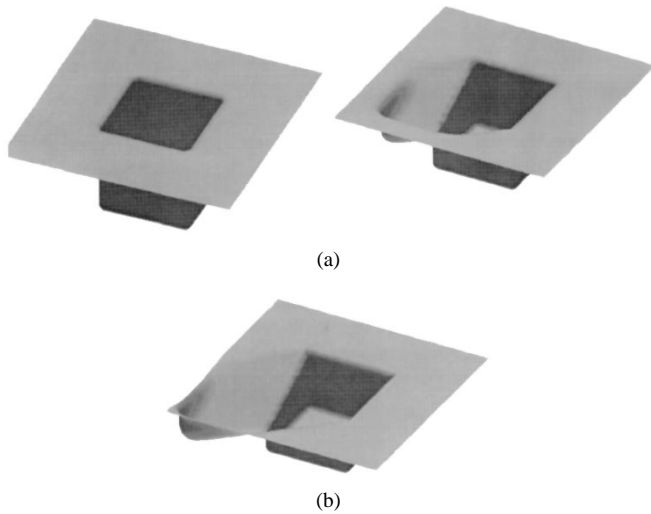
Fig. 14.   Directional etching into hole.

Fig. 15.   Source deposition into cavity.

the profile on the left first, and then as the shadowing wall is eaten away, continues to shear the left side of the profile.

3) Source Etching/Deposition: Here, we study source deposition into a two-dimensional trench with a cavity on the right (Fig. 15). We take a deposition source above a trench, where deposition material is emitted from a line source from the solid line above the trench. The deposition rate is the same in all directions, and the effects of shadowing are considered. The cavity is hidden from the deposition source, and grows very slowly; as the walls pinch toward each other, the seen visible angle decreases and the deposition rate in cavity slows zero. The calculation is performed on a grid with 160 cells in the horizontal direction and again a tube width of six cells on each side of the interface.

Next, we show how topology can change under the effects of etching, and study etching of a bridge, as a cartoon example. The bridge initially has a thin curtain stretched underneath it; the thickness of the curtain is smallest at the middle, [see Fig. 16(a)]. First the thin curtain is etched away, then the bridge connecting the two pillars is removed.

Fig. 16.   Source etching of bridge.

C. Non-Convex Flux Laws: Ion Milling

A more sophisticated set of examples arises in simulations (for example, of ion milling) in which the normal speed of the profile depends on the angle of incidence between the surface normal and the incoming beam. This yield function is often empirically fit from experiment, and has been observed to cause such effects as faceting at corners (see Leon *et al.* [17] and Katardjiev, Carter, and Nobes [16]). As shown in [3] and [4], such yield functions can often give rise to nonconvex Hamiltonians, in which case alternative schemes must be used.

As an example, consider an etching beam coming down in the vertical direction. In the cases under study here, the angle θ shown in Fig. 8 refers to the angle between the surface normal and the positive vertical. For this set of calculations, in order to focus on the geometry of sputter effects on shocks/rarefaction fan development, visibility effects are ignored. Following our usual notation, let $F(\theta)$ be the speed of the front in direction normal to the surface, and consider three different speed functions:
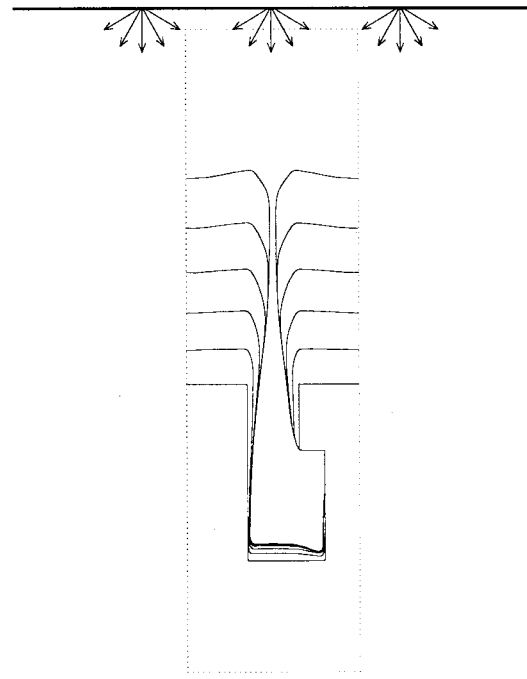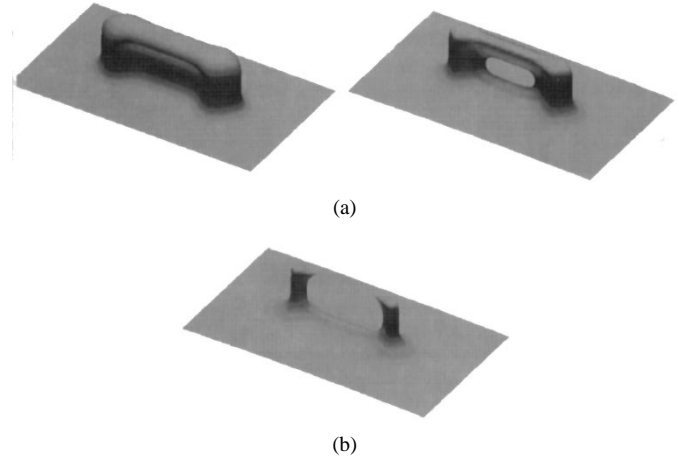
- $F(\theta) = 1$
- $F(\theta) = \cos(\theta)$
- $F(\theta) = [1. + 4\sin^2(\theta)]\cos(\theta)$.

The first case corresponds to isotropic etching. We shall now show that the third case leads to a nonconvex Hamiltonian. We have

$$\phi_t + F|\nabla\phi| = \phi_t + [(1+A)\cos\theta - A\cos^3\theta]|\nabla\phi|. \quad (24)$$

Noting that $\cos\theta = \phi_y/|\nabla\phi|$, some manipulation produces

$$\phi_t + H(\phi_x, \phi_y) = 0 \quad (25)$$

where the Hamiltonian H is now $H = (1 + A)\phi_y - A(\phi_y^3/|\nabla\phi|^2)$. This Hamiltonian is in fact nonconvex for $A > 0$.
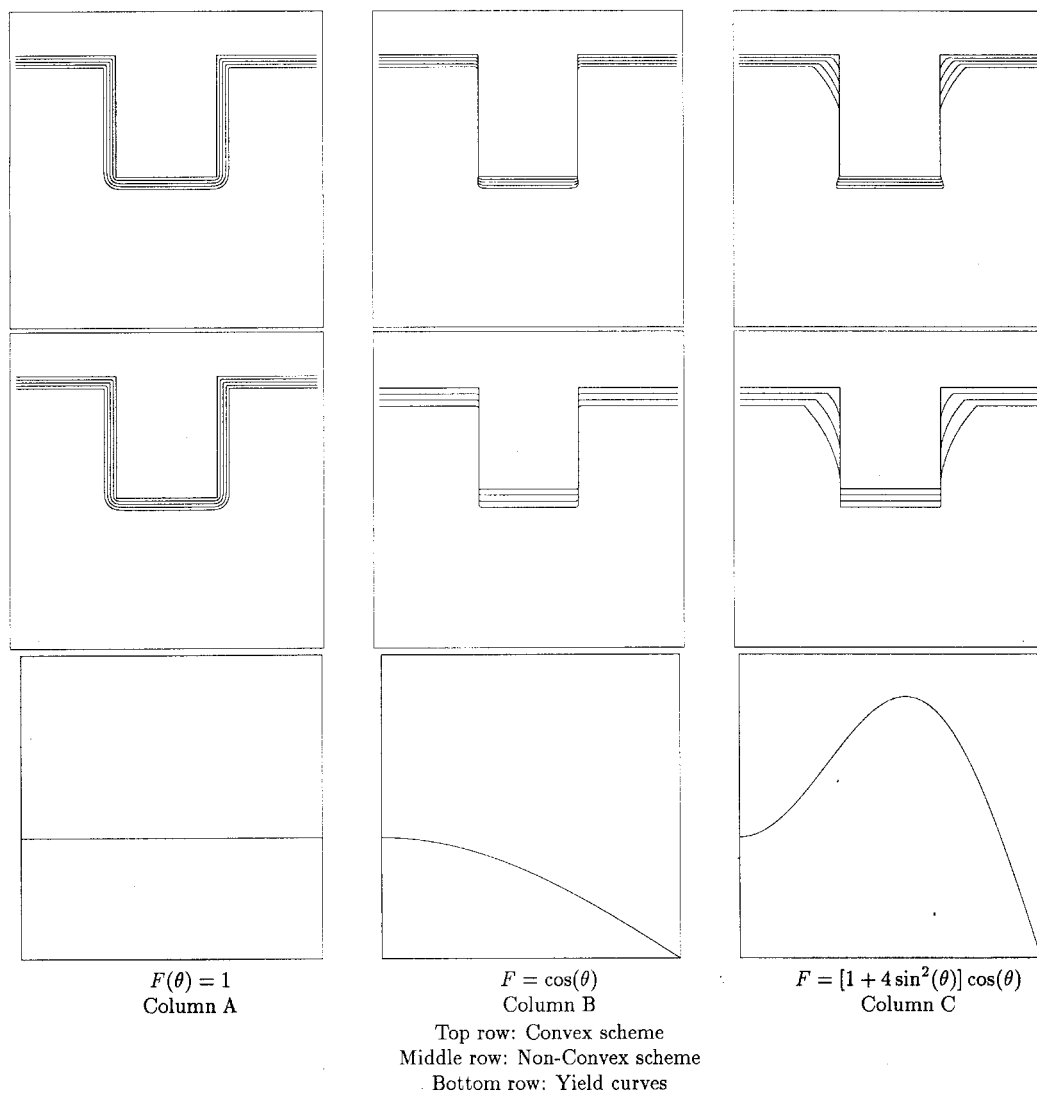
$F(\theta) = 1$
Column A

$F = \cos(\theta)$
Column B

$F = [1 + 4\sin^2(\theta)]\cos(\theta)$
Column C

Top row: Convex scheme
Middle row: Non-Convex scheme
Bottom row: Yield curves

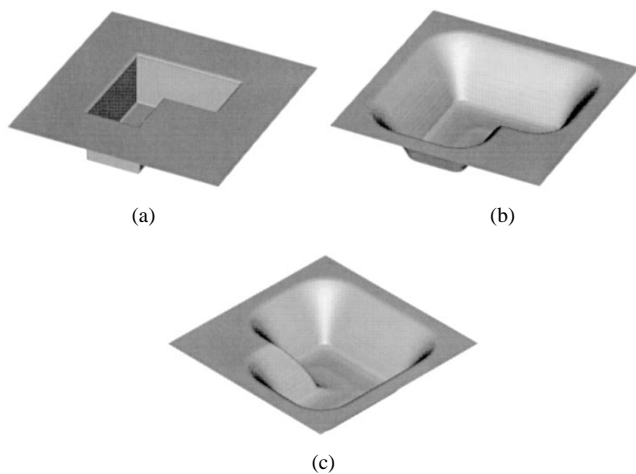Fig. 17. Ion-milling under various yield functions.

(a)

(b)

(c)

Fig. 18. Downward saddle under ion milling.

Thus, in the case of this nonconvex Hamiltonian, we must use the appropriate schemes given earlier. In Fig. 17, we show the results of applying both the convex and the nonconvex schemes. In Column A, the effects of purely isotropic motion

are shown, thus the yield function is $F = 1$. Located above the yield graph are the motions of a downwards square wave under etching. The top row is calculated using the convex scheme, and the second row using the nonconvex scheme. In Column B, the effects of directional motion are shown, thus the yield function is $F = \cos(\theta)$. In this case, the horizontal components on the profile do not move, and vertical components move with unit speed. In Column C, the effects of a yield function of the form $F = [1 + 4\sin^2(\theta)]\cos(\theta)$ are shown.

The results of these calculations are given in Fig. 17. The results show that the effects of angle dependent yield functions are pronounced. In Column A the isotropic rate produces smooth corners, correctly building the necessary rarefaction fans in outward corners and entropy-satisfying shocks in inward corners as discussed and analyzed in [32], [33]. In Column B, the directional rate causes the front to be essentially translated downwards, with minimal rounding of the corners. In Column C, the yield function results in faceting of inward corners where shocks form and sharp corners in the construction of rarefaction fans. We note that the application of the convex scheme to the nonconvex Hamiltonian in Column C
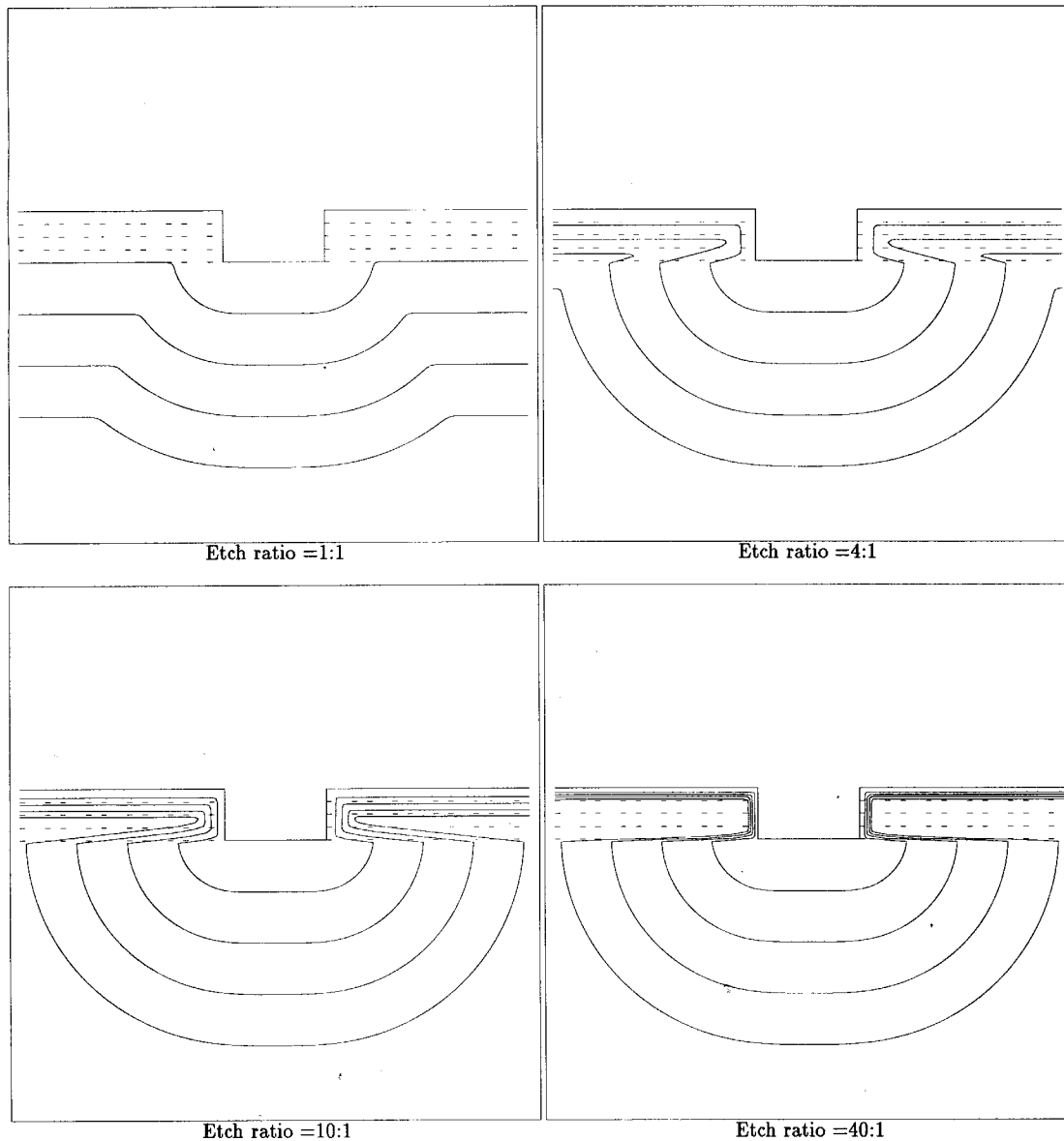
Fig. 19.   Etch ratio = bottom material rate to top material rate.

leads to incorrect results, whereas application of the nonconvex scheme produces the expected answer.

A three-dimensional ion-milling simulation into an indented saddle surface is shown in Fig. 18.

D. Strongly Discontinuous Etch Rates/Simultaneous Etching and Deposition

Next, we study the effects of etching through different materials. In this example, the etch rates are discontinuous, and hence sharp corners develop in the propagating profile. The results of these calculations are show in Fig. 19. A top material masks a lower material, and the profile etches through the lower material first and underneath the upper material. The profile depends on the ratio of the etch rates. In Fig. 19(a), the two materials have the same etch rate, and hence the front simply propagates in its normal direction with unit speed, regardless of which material it is passing through. In

Fig. 19(b), the bottom material etches four times faster that the top; in Fig. 19(c), the ratio is ten to one. Finally, in Fig. 19(d), the ratio is 40:1, in which case the top material almost acts like a mask.

Next, we perform a parameter study of simultaneous etching and deposition is taken from [5], using speed function

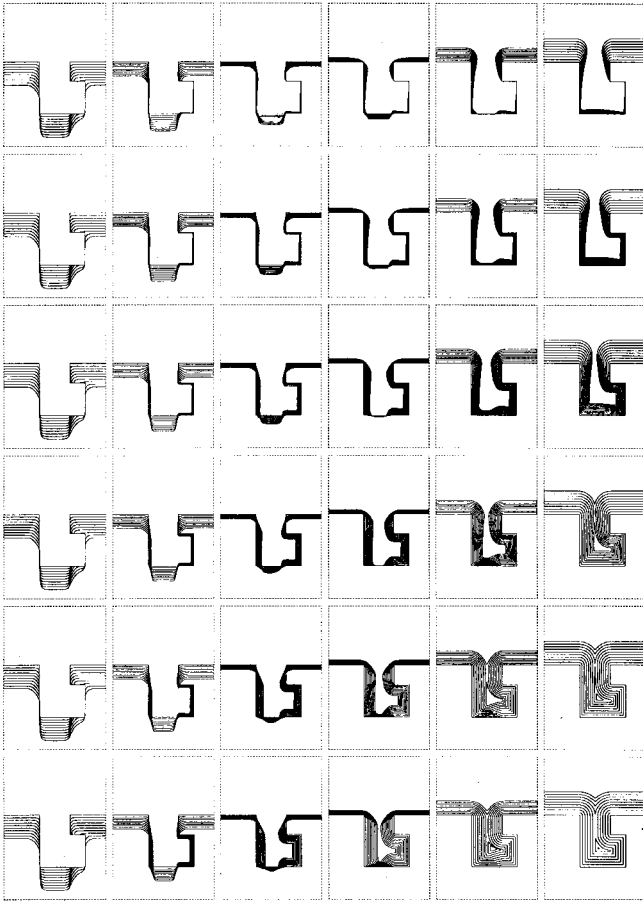$$F = (1 - \alpha)F_{etch} + \alpha F_{Deposition} \qquad (26)$$

where

$$F_{etch} = (5.2249 \cos \theta - 5.5914 \cos^2 \theta \\ + 1.3665 \cos^4 \theta) \qquad (27)$$

$$F_{Deposition} = \beta F_{Isotropic} + (1 - \beta)F_{Source}. \qquad (28)$$

Visibility effects are considered in all terms except isotropic deposition. Fig. 20 shows the results of varying α and β between 0 and 1.

For details and additional simulations, see [3]–[5].

$$F = (1 - \alpha)F_{etch} + \alpha F_{Deposition}$$

$$F_{etch} = (5.2249 \cos \theta - 5.5914 \cos^2 \theta + 1.3665 \cos^4 \theta) \cos \theta$$

$$F_{Deposition} = \beta F_{Isotropic} + (1 - \beta)F_{Source}$$

α Increases from left to right
β Increases from top to bottom

Fig. 20. Simultaneous etching and deposition.

E. Ion-Induced Re-Deposition

Next, we show a combination of effects. Fig. 21, taken from [5], includes a combination of ion-milling (using a nonconvex sputter law) and ion-induced sputtered re-deposition, together with conformal deposition and direct deposition. In both calculations, the direct deposition term includes the effect of visibility, and the conformal deposition is isotropic. In Fig. 21(a), the ion-induced sputter re-deposition coefficient is set to 1.0, which means that there is no re-deposition. In Fig. 21(b), which requires integration over the entire profile as well as the source, the re-deposition coefficient is set to 1/2 re-deposition occurs during the etching process, resulting in considerable rounding of the sharp corners.

F. Re-Emission; Low Sticking Coefficients

Next, we show an example, taken from [5], that shows re-emission for various values of the sticking coefficient; this requires solving the associated integral equation which computes the total flux from both the direct source and re-emitted from the evolving surface. In Fig. 22, we show a
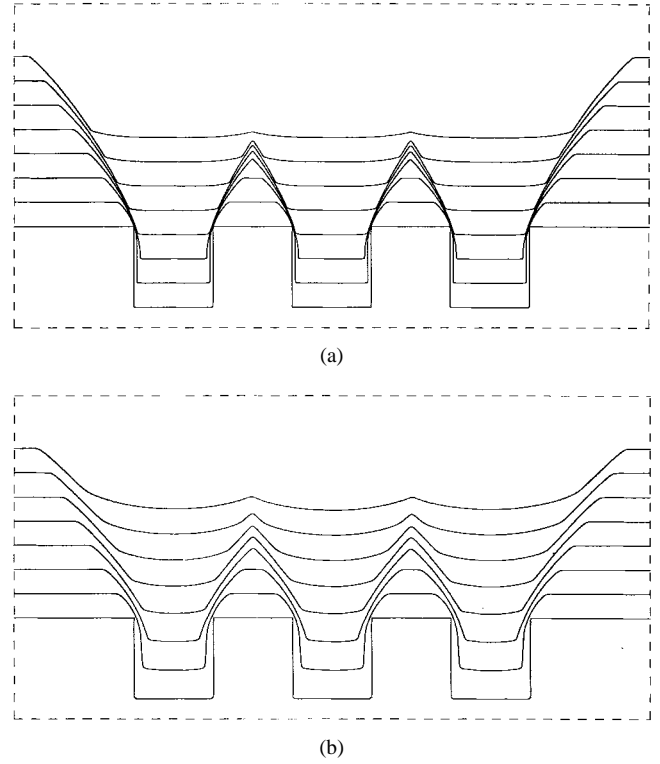

(a)

(b)

Fig. 21. Combination of ion-milling, direct deposition, and conformal deposition.
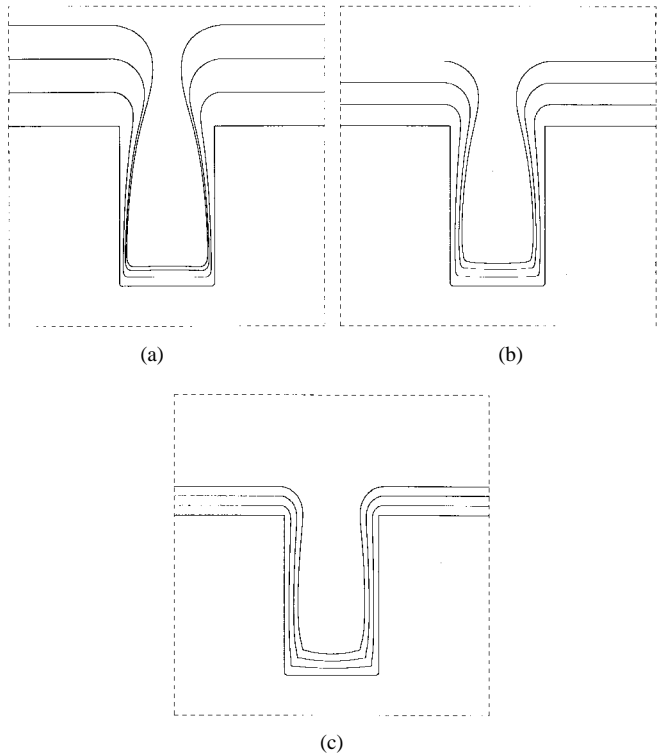

(a)   (b)

(c)

Fig. 22. Source deposition: re-emission effects under various sticking coefficients.

trench subject to deposition from a line source, including the effects of visibility. In Fig. 22(a), the sticking coefficient is 0.7, and most of the particles stick. In Fig. 22(b), the sticking
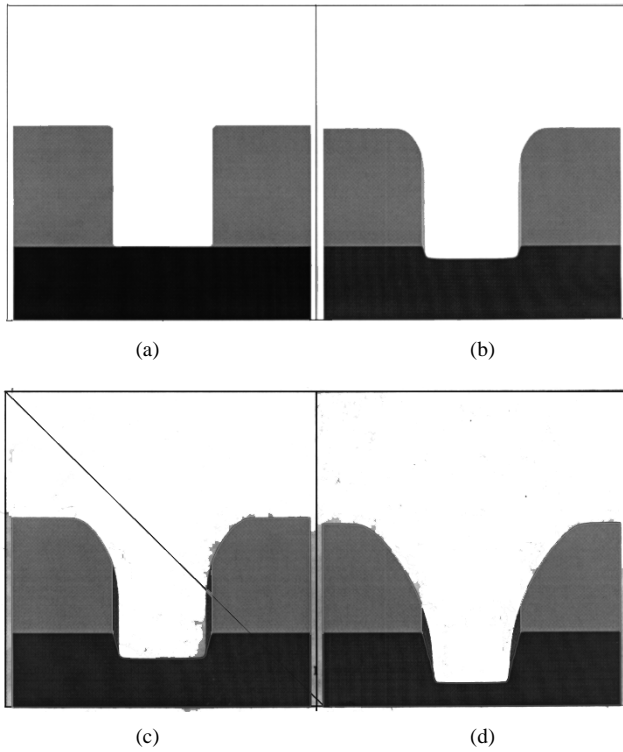
Fig. 23. Combination of isotropic deposition of thin layer and non-convex sputter etching of materials: Time Sequence.

coefficient is 0.45, and in Fig. 22(c) the sticking coefficient is 0.2. In the last simulation, the result more closely resembles isotropic deposition due to the large amount of re-emitted material.

G. Thin Layers/Triple Points, and Multiple 3-D Effects

We end with two additional simulations, designed to show the versatility of this approach. We begin with a study of thin layers and triple points, imagine an initial block, in which a mask covers a substrate, and envision a simultaneous etch and deposition process. We imagine that one material (which will be shown as light gray) is isotropically deposited on both the mask (shown in dark gray) and substrate (shown in black). At the same time that this material is being deposited, it is being etched under an ion-milling/sputter law, such that the etch rate in the substrate is twice as fast as the etch rate in the mask. The ion-milling sputter law is of the non-convex variety, and thus promotes faceting. We have

$$F = F_{Isotropic Deposition} + F_{Sputter Etching} \qquad (29)$$

$$F_{Isotropic Deposition} = .5 \qquad (30)$$

$$F_{Sputter Etching} = Factor(x) * (1. + 4 sin^2 \theta) * \cos\theta \qquad (31)$$

- $Factor(x) = 1.0$ if in dark gray material (Mask).
- $Factor(x) = 2.0$ if in black material (Substrate).

In Fig. 23, we show the sequence of profile evolution under these effects. We note the development of the thin nano-layer which covers the side walls, but is fully etched away along the top and the bottom; we also note the existence of evolving
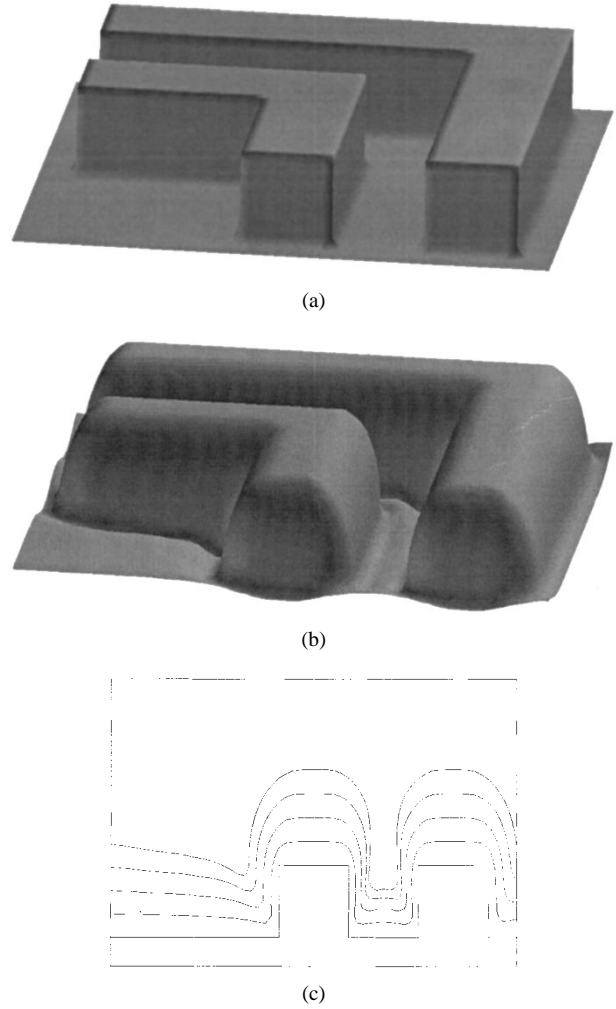

(a)

(b)

(c)

Fig. 24. 3-D Evolution: Cosine Distribution/Sticking Coefficient .1. (a) Initial position. (b) Time evolution. (c) 2-D cross section.

triple points. We stress that the grid used for this calculation is *significantly larger* than the size of the nano-layer; thus our algorithms provide for significant sub-grid resolution without resorting to adaptive mesh technology, see [41] for details of this technology.

Finally, we perform a study which balances source distribution using an angular flux cosine dependence with a combination of two cosine flux deposition sources. That is, let the $Flux(x)$ received at a point x on the surface emitted from a point y on the source be given by

$$Flux(x) = \cos^5(\theta_1)\cos(\theta_2) + \cos(\theta_1)\cos(\theta_2) \qquad (32)$$

where θ_1 is the angle that the vector v from x to y makes with the normal at x, and θ_2 is the angle that the vector v makes with the vertical. This flux is integrated over the entire source to obtain the speed function F at the point x. The second deposition term is given a sticking coefficient of .1, thus we also consider the effects of re-deposition. Results are shown after some time evolution in Fig. 24(b); a two-dimensional cross-sectional cut is shown in Fig. 24(c).

Detailed discussion of these effects, including surface diffusion, may be found in [5].

VI. Summary and Future Work

The numerical method presented in this paper can be used for a wide variety of three-dimensional simulations in etching, deposition and lithography; the method naturally takes into account such effects as incident angles, masks, yield functions, visibility, and anisotropy on the surface motion. Due to the use of conservative upwind schemes, the method selects the correct entropy condition and maintains sharp corners where shocks in the tangent occurs; conversely, the correct rarefaction fan solution is built at outward-facing corners. The method is second order accurate in space and time in the motion of the front. By using the narrow band approach, the method is of the same computational work as cell and marker particle methods; that is, the work is a constant times the number of points which characterize the evolving front. In the case of problems in which the speed function depends only on independent variables, the fast marching level set method for the stationary formulation provides an extremely fast technique.

In [5], we focus on additional terms, and provide a wide collection of examples.

Acknowledgment

References

[1] D. Adalsteinsson, R. Kimmel, R. Malladi, and J. A. Sethian, "Fast marching methods for computing the solutions to static Hamilton–Jacobi equations," CPAM Rep. 667, Univ. of California, Berkeley, *SIAM J. Num. Anal.,* Feb. 1996, submitted for publication.

[2] D. Adalsteinsson and J. A. Sethian, "A fast level set method for propagating interfaces," *J. Comp. Phys.,* vol. 118, pp. 269–277, May 1995.

[3] ———, "A unified level set approach to etching, deposition and lithography I: Algorithms and two-dimensional simulations," *J. Comp. Phys.,* vol. 120, pp. 128–144, 1995.

[4] ———, "A unified level set approach to etching, deposition and lithography II: Three-dimensional simulations," *J. Comp. Phys.,* vol. 122, pp. 348–366, 1995.

[5] ———, "A unified level set approach to etching, deposition and lithography III: Complex simulations and multiple effects," *J. Comp. Phys.,* 1996, submitted for publication.

[6] T. S. Cale and G. B. Raupp, "Free molecular transport and deposition in cylindrical features," *J. Vac. Sci. Technol. B,* vol. 8, no. 4, pp. 649–655, 1990.

[7] ———, "Free molecular transport and deposition in long rectangular trenches," *J. Appl. Phys.,* vol. 68, no. 7, pp. 3645–8652, 1990.

[8] ———, "A unified line-of-sight model of deposition in rectangular trenches," *J. Vac. Sci. Technol. B* vol. 8, no. 6, pp. 1242–1248, 1990.

[9] Y. Chen, Y. Giga, and S. Goto, "Uniqueness and existence of viscosity solutions of generalized mean curvature flow equations," *J. Differ. Geom.,* vol. 33, p. 749, 1991.

[10] D. L. Chopp, "Computing minimal surfaces via level set curvature flow," *J. Comp. Phys.,* vol. 106, pp. 77–91, 1993.

[11] D. L. Chopp and J. A. Sethian, "Flow under curvature: Singularity formation, minimal surfaces, and geodesics," *J. Exper. Math.,* vol. 2, no. 4, pp. 235–255, 1993.

[12] L. C. Evans and J. Spruck, "Motion of level sets by mean curvature I," *J. Differ. Geom.,* vol. 33, p. 635, 1991.

[13] M. Falcone, "The minimum time problem and its applications to front propagation, in 'Motion by mean curvature and related topics,'" in *Proc. Int. Conf. Trento, 1992.* New York: Walter de Gruyter, 1994.

[14] M. Falcone, T. Giorgi, and P. Loretti, "Level sets of viscosity solutions: Some applications to fronts and Rendez–Vous problems," *SIAM J. Appl. Math.,* vol. 54, no. 5, pp. 1335–1354, 1994.

[15] J. J. Helmsen, "A comparison of three-dimensional photolithography development methods," Ph.D. dissertation, Dept. EECS, Univ. California, Berkeley, 1994.

[16] I. V. Katardjiev, G. Carter, and M. J. Nobes, "Precision modeling of the mask-substrate evolution during ion etching," *J. Vac. Sci. Technol. A,* vol. 6, no. 4, pp. 2443–2450, 1988.

[17] F. A. Leon, S. Tazawa, K. Saito, A. Yoshi, and D. L. Scharfetter, "Numerical algorithms for precise calculation of surface movement in 3-D topography simulation," in *1993 Int. Workshop on VLSI Process and Device Modeling (1993 VPAD).*

[18] R. Malladi and J. A. Sethian, "Image processing via level set curvature flow," *Proc. Nat. Acad. Sci.,* vol. 92, pp. 7046–7050, July 1995.

[19] R. Malladi, J. A. Sethian, and B. C. Vemuri, "Shape modeling with front propagation: A level set approach," *IEEE Trans. Pattern. Anal. Machine. Intell.,* vol. 17, pp. 158–175, Feb. 1995.

[20] J. P. McVittie, J. C. Rey, A. J. Bariya, and others, "SPEEDIE: A profile simulator for etching and deposition," in *Proc. SPIE—The Int. Soc. Opt. Eng.,* 1991, vol. 1392, pp. 126–38.

[21] W. Mulder, S. J. Osher, and J. A. Sethian, "Computing interface motion in compressible gas dynamics," *J. Comp. Phys.,* vol. 100, pp. 209–228, 1992.

[22] W. Noh and P. Woodward, in *Proc. Fifth Int. Conf. Fluid Dynamics,* A. I. van de Vooran and P. J. Zandberger, Eds. New York: Springer-Verlag, 1976.

[23] S. Osher and J. A. Sethian, "Fronts propagating with curvature dependent speed: Algorithms based on Hamilton–Jacobi formulation," *J. Comp. Phys.,* vol. 79, pp. 12–49, 1988.

[24] W. H. Press, S. A. Teukolsky, W. T. Vetterling, and B. P. Flannery, *Numerical Recipes.* New York: Cambridge Univ. Press, 1988

[25] E. G. Puckett, "A volume-of-fluid interface tracking algorithm with applications to computing shock wave refraction," in *Proc. 4th Int. Symp. Computational Fluid Dynamics,* Davis, CA, 1991

[26] J. C. Rey, L.-Y. Cheng, J. P. McVittie, and K. C. Saraswat, "Monte Carlo low pressure deposition profile simulations," *J. Vac. Sci. Technol. A,* vol. 9, no. 3, pt. 1, pp. 1083–1087, May/June 1991.

[27] C. Rhee, L. Talbot, and J. A. Sethian, "Dynamical study of a premixed V flame," *J. Fluid Mech.,* vol. 300, pp. 87–115, 1995.

[28] E. Rouy and A. Tourin, "A viscosity solutions approach to shape-from-shading," *SIAM J. Numer. Anal.,* vol. 29, no. 3, pp. 867–884, 1992.

[29] E. W. Scheckler, Ph.D. dissertation, Dept. EECS, Univ. California, Berkeley, 1991.

[30] E. W. Scheckler, K. K. H. Toh, D. M. Hoffstetter, and A. R. Neureuther, "3D lithography, etching and deposition simulation," in *Symp. VLSI Tech.,* Oiso, Japan, 1991, pp. 97–98.

[31] R. Sedgewick, *Algorithms.* Reading, MA: Addison-Wesley, 1988.

[32] J. A. Sethian, "An analysis of flame propagation," Ph.D. dissertation, Dept. Mathematics, Univ. California, Berkeley, 1982.

[33] ———, "Curvature and the evolution of fronts," *Commun. Math. Phys.,* vol. 101, pp. 487–499, 1985.

[34] ———, "Numerical methods for propagating fronts," in *Variational Methods for Free Surface Interfaces,* P. Concus and R. Finn, Ed. New York: Springer-Verlag, 1987.

[35] ———, "Numerical algorithms for propagating interfaces: Hamilton–Jacobi equations and conservation laws," *J. Differ. Geom.,* vol. 31, pp. 131–161, 1990.

[36] ———, "Curvature flow and entropy conditions applied to grid generation," *J. Comp. Phys.,* vol. 115, pp. 440–454, 1994.

[37] ———, "Level set techniques for tracking interfaces; fast algorithms, multiple regions, grid generation and shape/character recognition," in *Proc. Second Trento Conf. Mean Curvature Motion,* July 1994.

[38] ———, "Algorithms for tracking interfaces in CFD and material science," *Ann. Rev. Comp. Fluid Mech.,* 1995.

[39] ———, "A fast marching level set method for monotonically advancing fronts," *Proc. Nat. Acad. Sci.,* vol. 93, no. 4, 1996.

[40] ———, "A review of the theory, algorithms, and applications of level set methods for propagating interfaces," *Acta Numerica,* 1995, in press.

[41] ———, *Level Set Methods: Evolving Interfaces in Geometry, Fluid Mechanics, Computer Vision and Material Science.* New York: Cambridge Univ. Press, 1996.

[42] J. A. Sethian and J. D. Strain, "Crystal growth and dendritic solidification," *J. Comp. Phys.,* vol. 98, pp. 231–253, 1992.

[43] V. K. Singh, S. G. Shaqfeh, and J. P. McVittie, "Simulation of profile evolution in silicon reactive ion etching with re-emission and surface diffusion," *J. Vac. Sci. Tech. B,* vol. 10, no. 3, pp. 1091–1104, 1993.

[44] Technology Modeling Associates, "Three-dimensional photolithography simulation with depict 4.0," Technology Modeling Assoc., Internal Doc., Jan. 1996.

[45] K. K. H. Toh, Ph.D. dissertation, Dept. EECS, Univ. California, Berkeley, 1990.

[46] K. K. H. Toh and A. R. Neureuther, "Three-dimensional simulation of optical lithography," in *Proc. SPIE, Optical/Laser Microlithography IV,* 1991, vol. 1463, pp. 356–367.

[47] J. Zhu and J. A. Sethian, "Projection methods coupled to level set interface techniques," *J. Comp. Phys.,* vol. 102, pp. 128–138, 1992.
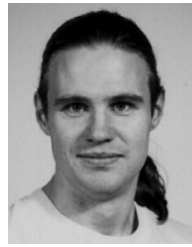
David Adalsteinsson received the B.S. degree in mathematics from the University of Iceland in 1990, and the Ph.D. degree in applied mathematics from the University of California, Berkeley, in 1995.

He is currently working at the Lawrence Berkeley National Laboratory, University of California, Berkeley. His research interests are focused on front propagation and fast computational methods.

James A. Sethian is a Professor of Mathematics at the University of California at Berkeley, and the Head of the Mathematics Department, Lawrence Berkeley National Laboratory.